Effects of Oxygen Transport on 3-D Human Mesenchymal Stem Cell Metabolic Activity in Perfusion and Static Cultures: Experiments and Mathematical Model

Feng Zhao, Pragyansri Pathi, Warren Grayson, Qi Xing, Bruce R. Locke, and Teng Ma*

Department of Chemical and Biomedical Engineering, FAMU-FSU College of Engineering, Florida State University, Tallahassee, Florida 32310

Human mesenchymal stem cells (hMSCs) have unique potential to develop into functional tissue constructs to replace a wide range of tissues damaged by disease or injury. While recent studies have highlighted the necessity for 3-D culture systems to facilitate the proper biological, physiological, and developmental processes of the cells, the effects of the physiological environment on the intrinsic tissue development characteristics in the 3-D scaffolds have not been fully investigated. In this study, experimental results from a 3-D perfusion bioreactor system and the static culture are combined with a mathematical model to assess the effects of oxygen transport on hMSC metabolism and proliferation in 3-D constructs grown in static and perfusion conditions. Cells grown in the perfusion culture had order of magnitude higher metabolic rates, and the perfusion culture supports higher cell density at the end of cultivation. The specific oxygen consumption rate for the constructs in the perfusion bioreactor was found to decrease from 0.012 to 0.0017 μmol/10^6 cells/h as cell density increases, suggesting intrinsic physiological change at high cell density. BrdU staining revealed the noneven spatial distribution of the proliferating cells in the constructs grown under static culture conditions compared to the cells that were grown in the perfusion system. The hypothesis that the constructs in static culture grow under oxygen limitation is supported by higher $Y_{L/G}$ in static culture. Modeling results show that the oxygen tension in the static culture is lower than that of the perfusion unit, where the cell density was 4 times higher. The experimental and modeling results show the dependence of cell metabolism and spatial growth patterns on the culture environment and highlight the need to optimize the culture parameters in hMSC tissue engineering

Introduction

Current clinical progress gives an indication of the potential of human mesenchymal stem cells (hMSCs) for treating a wide range of diseases including osteogenesis imperfecta (*1*, *2*), stroke (*3*, *4*), and heart failure (*5*). The potential of human stem cells in therapeutic applications depends on their high proliferative capacity, maintenance of progenicity, and plasticity. To utilize hMSCs in clinical practice, a major obstacle is to expand them in 3-D scaffolds to reach tissue-like cellularity while retaining their abilities to differentiate into specific tissue types. This requires high yields for hMSC isolation, as well as the improbable combination of high expansion rates, maintenance of primitiveness, and formation of desired tissue structure and characteristics. To achieve a high cell proliferation rate and subsequent differentiation of cellular constructs, a perfusion bioreactor system is utilized to ensure sufficient oxygen and nutrient delivery.

Bioreactor systems have been developed as effective tools to provide suitable microenvironments for supporting functional engineered tissue constructs and 3-D tissue ex vivo development (*6*−*12*). Uniform tissue development requires timely delivery of nutrients and oxygen, and removal of metabolites. Various types of bioreactors have been developed to achieve this goal. Stirred flasks have been used to reduce the concentration boundary layer at the construct surface by mixing oxygen and nutrients throughout the medium (*13*, *14*). Rotating-wall vessel (RWV) bioreactors were designed to generate a dynamic laminar flow and consequently reduce diffusion limitations of nutrients and wastes while producing low levels of shear (*9*, *15*). Perfusion bioreactors meanwhile have proven to be valuable tools for enhancing cell survival, growth, and function by perfusing medium either through or around semipermeable hollow fibers (*16*) or cell-seeded porous 3D scaffolds (*17*) to reduce mass transfer limitations at the construct periphery and within its internal pores. Additionally, fluid flow and shear stress have been found to affect cell growth by increasing the mineralized matrix deposition in the 3-D perfusion culture of marrow stromal osteoblast cells, indicating that the mechanical environment influences 3-D tissue formation (*7*, *18*). Compared to the static 3-D cultures conducted in the standardized CO_2 incubator, the perfusion bioreactor

* To whom correspondence should be addressed. Tel: (850) 410-6558. Fax: (850) 410-6150. E-mail: teng@eng.fsu.edu.

10.1021/bp0500664 CCC: $30.25
Published on Web 06/25/2005

system provides a dynamic and efficient culture environment with respect to fluid flow and nutrient delivery. The presence of media flow in the perfusion system also removes detached cells, preventing the noneven distribution of cell mass in the constructs. In a prior study a perfusion bioreactor with integrated seeding and long-term culture functions for producing 3-D engineered tissue constructs was developed in which perfusion through and around the constructs are combined in a single unit for seeding and culturing, respectively (*19*). It was found that hMSCs grown in perfusion conditions exhibited more homogeneous spatial growth patterns compared to their counterparts in the 3-D poly(ethylene terephthalate) (PET) constructs (*19*).

In this study, hMSC growth kinetics and spatial growth patterns, metabolism, and oxygen consumption in static and perfusion cultures were investigated and compared. Oxygen transport is modeled on the basis of experimental parameters and the higher levels of the oxygen concentrations found throughout the culture period in the perfusion unit support the experimental observations of uniform cell growth patterns and significantly higher final cell density in the construct. The experimental and modeling results from this study provide insight into the role of oxygen transport in hMSC proliferation and metabolism in 3-D constructs, which is important in optimizing culture conditions for hMSC tissue engineering.

Materials and Methods

Cell Culture and Matrices. Human mesenchymal stem cells (hMSCs) were obtained following a method outlined in prior publications (*19*, *20*). Briefly, bone marrow aspirates of about 2 mL were drawn from healthy donors ranging in age from 19 to 49 years under an Institutional Review Board approved protocol. Plastic adherent nucleated cells were separated from the aspirate and cultured as previously described (*21*, *22*). These cells were expanded using α-MEM (Life Technologies, Rockville, MD) with 10% FBS (Life Technologies, Rockville, MD) and 1% Penicillin/Streptomycin (Life Technologies, Rockville, MD) and grown at 37 °C and 5% CO_2.

The PET matrices were treated as previously described (*23*) and compressed to a porosity of 89%. The matrices were cut into disks with a diameter of 1.6 cm and a thickness of 1.2 mm for perfusion culture, and a diameter of 1.2 cm and a thickness of 1.2 mm for static culture.

Static Culture. Approximately 2×10^6 cells were seeded onto the PET matrices via depth filtration (*19*, *20*). The PET matrices were then transferred to 12-well plates, with one matrix per well in 3 mL of media. Media were changed every 2 days.

Perfusion Culture. A perfusion bioreactor system with modular perfusion chambers and integrated seeding loop was set up as described previously (*19*). Four chambers were used in parallel in this study. The seeding loop was utilized to inject 8.0×10^5 cells in each chamber at a flow rate of 0.1 mL/min. After seeding, the cultures were maintained for up to 40 days. During this time media was fed to the upper and lower portions of each chamber at a flow rate of 0.1 mL/min.

Oxygen and Glucose Consumption. Oxygen tension and pH values of the bioreactor system were maintained by passing a blend of air and CO_2 through the media container. Medium samples were collected through sampling ports located at the inlets and outlets of the perfusion chambers and the dissolved oxygen tension was analyzed immediately using a blood gas analyzer (pHOx, Nova Biomedical, Waltham, MA). Metabolic activities were monitored by measuring glucose and lactate concentrations using an YSI 2500 Biochemistry Select Analyzer (Yellow Springs, OH).

DNA Assays. Cell numbers in the PET matrices were determined by DNA assay following a method reported in a prior publication (*24*). Briefly, a DNA standard was prepared by dissolving salmon testes DNA (Sigma, St. Louis, MO) in TEX (10 mM Tris, 1 mM EDTA, 0.1% Triton X-100) and its concentration was measured using a spectrophotometer. A serial dilution was prepared and used to give a standard curve for each assay. Constructs were lysed using TEX with 0.1 mg/mL proteinase *K* (Sigma, St. Louis, MO) at 50 °C overnight. Samples (100 μL) were placed in triplicate into a 96-well plate and 100 μL of Picogreen (Molecular Probes, Eugene, OR) was added to each well. The plate was then incubated at 37 °C for 10 min in the dark and then read on a fluorescent plate reader (Fluoro Count, PerkinElmer, Boston, MA). At the time of seeding operation, three aliquots of the seeding cell suspension were collected and centrifuged to obtain pellets and, as with the scaffolds, digested with Proteinase *K* solution. These samples served as basis for calculations of the average DNA content. The hMSC was thereby found to contain average DNA level of 9.3 pg/cell. The cell number in the constructs was calculated on the basis of the total amount of DNA contained in each construct sample and the average DNA content of hMSCs, and the cell density was determined by averaging the cell number by the matrix volume.

Bromodeoxyuridine (BrdU) Staining. The cell constructs were cultured in media supplemented with BrdU (Sigma, St. Louis, MO) (10 μM) for 20 h. They were then washed with TBS (100 mM Tris.Cl, 150 mM NaCl, pH 7.5) and fixed with 70% ethanol (−20 °C) for 10 min, denatured with 2 N HCl/0.5% Triton X-100 in TBS for 20 min at room temperature and rinsed with 0.025% Triton X-100 in TBS. The constructs were blocked using TBS with 1% BSA and 10% FBS at room temperature for 2 h and then incubated with anti-BrdU conjugated to FITC (Abcam, Cambridge, MA) overnight at 4 °C. Cells were stored in TBS and stained with PI before viewing with a Zeiss 510 confocal microscope. Two constructs were used for the BrdU staining, and 25% of the construct surface was investigated. Three arbitrary view fields were chosen at the surface of the constructs within the depth of 50 μm in each. The percentage of BrdU positive cells were calculated as the number of BrdU positive cells divided by the total number of cells obtained from PI staining and the data were pooled for statistical analysis.

Statistical Analysis. The data for perfusion bioreactor system are representative data from at least three independent runs under the same condition. For static culture, at least triplicate sets of matrices were used for each data point. Student's *t* test was used for statistical analysis and the statistical significance was set at $p < 0.05$.

Mathematical Model Development. Mathematical models for oxygen transport and reaction are developed for perfusion and static culture units to assess the importance of perfusion flow on cell proliferation and metabolism.

Perfusion Reactor Design (Unit 1). Unit 1 represents the 3-D perfusion chamber as shown schematically in Figure 1a (refer to ref 19 for details of design and setup). The chamber is cubical in shape, 10 cm in length, 2.5 cm in width, and 12 mm in depth. An impermeable PC panel with a thickness of 3.0 mm equally separates

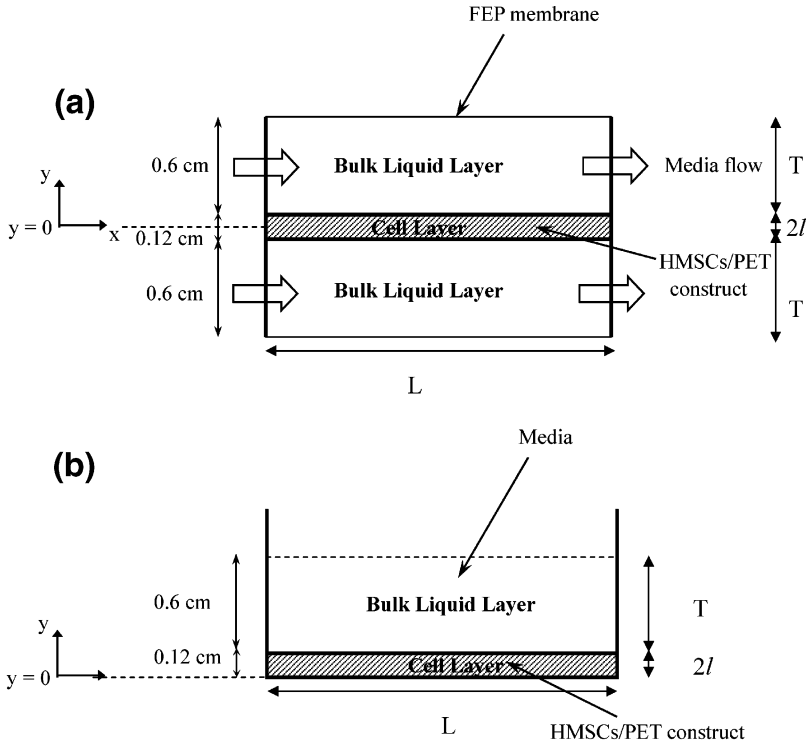

Figure 1. Schematic of systems used to develop mathematical model for oxygen variation in static and perfusion systems: (a) perfusion culture, (b) static culture.

the perfusion chamber into upper and lower compartments. Three grooves of 1.6 cm diameter are machined on the central panel along the length of the perfusion chambers. The disks (1.2 mm thick) of the PET matrix were tucked into the grooves. Aluminum lid frames and stainless bolts were used to fix the transparent FEP membranes (thickness 130 μm) on both sides of the PC body. Cells are grown in the 3-D matrix and form what is termed the "cell layer" of the chamber. This cell layer is assumed to be a rectangle for modeling simplicity. The medium that supplies nutrients to cells in the cell layer flows through the perfusion chambers above and below the matrix and is termed the "bulk liquid layer".

Oxygen transports through the bulk liquid layer by convection and diffusion. Nutrients are supplied by flow through either a once through mode or by recirculation of the bulk liquid layer medium (*19*). Diffusion of oxygen from the incubator occurs through the FEP membrane into the perfusion chambers. In the cell layer oxygen is delivered by diffusive transport only. Convective oxygen supply inside the construct is neglected because of the relatively large restrictions to flow in the matrix. The two perfusion chambers above and below the matrix are identical with respect to flow and resistances. Clearly the absence of flow in the cell layer prevents flow restrictions on cell growth by shear or other mechanical forces and promotes adhesion of the cells to the matrix surface.

Static Culture Design (Unit 2). Unit 2 (Figure 1b) was used to model the static culture system in order to compare with the flow reactor Unit 1. This unit used for the model is a rectangular block 10 cm long, 2.5 cm wide, and 13.2 mm thick. The 3-D PET porous matrix (1.2 mm thick) is placed on the bottom of the reactor and forms the "cell layer". Medium supplying nutrients (oxygen) above the matrix forms the "bulk liquid layer". The mode of oxygen supply to the cells in the cell layer is only by diffusion through the stagnant liquid layer above the construct. Transport of oxygen in the cell layer is also by diffusion only. In addition to the absence of convection in the bulk liquid layer of Unit 2, the surface area of oxygen transport to the construct is also reduced to one-half of that in the perfusion bioreactor (Unit 1), reducing the amount of oxygen delivered to meet cell demands.

Model Equations.

Unit 1 (Perfusion Reactor). For the model development of Unit 1, only half of the reactor is considered due to symmetry. The species continuity equations describing the spatial and temporal variations of oxygen concentration are written for both the bulk liquid layer and the cell layer. The method of volume averaging was used to develop a single species continuity equation for the multiphase cell layer made up of cells and medium solution (*25*–*29*, *31*). It can be noted that the overall reactor model was solved in two dimensions (length and depth) since variation over the width are small compared to the length and depth.

Bulk Liquid Layer. The molar species continuity equation describing the oxygen concentration variation in the liquid layer in space and time is written as

$$\frac{\partial c}{\partial t} = (\nabla D_\beta \nabla c) - v_x \nabla c \qquad (1)$$

where c is the nondimensional oxygen concentration in the bulk liquid layer (the oxygen concentration terms are nondimensionalized by dividing the oxygen concentration at all point in space and time with the dissolved oxygen concentration in equilibrium with air (C_o = 20% oxygen or 152 mmHg or 2.10 $\times$ 10^{-7} mol/cm^3) and D_β is the diffusion coefficient of oxygen in the bulk liquid phase. The one-dimensional flow is oriented along the reactor length (x-direction) and is assumed to be laminar (Re = 0.28 corresponding to flow rate of 0.1 mL/min). The velocity profile is given as

$$v_x = \frac{6v_{ave}}{T^2}[(T + 2l)y - (y^2) - (l^2 + Tl)] \qquad (2)$$

where v_{av} is the average velocity of medium flow in the

perfusion chamber (bulk liquid layer), y is the direction perpendicular to the direction of flow, l is half the height of the matrix (cell layer), and T is the height of the liquid layer in the bioreactor.

Cell Layer. The cell layer is a two-phase region made up of cells and the liquid nutrient medium. The method of volume averaging is used to obtain a single continuity equation to describe mass transport by diffusion and consumption of oxygen by cells in the two phases (*25*−*27*, *31*). The averaged species continuity equation in the cellular construct is written as

$$\frac{\partial c}{\partial t} = \nabla D_{\text{eff}} \nabla c - \frac{Q_{\text{m}} K_{\text{eq}} \epsilon_\gamma c}{\frac{K_{\text{m}}}{C_{\text{o}}} + K_{\text{eq}} c \epsilon_\gamma} \tag{3}$$

where c is the nondimensional oxygen concentration in the construct, D_{eff} is the effective diffusion coefficient, ϵ_γ is the cell volume fraction, and K_{eq} is the equilibrium coefficient for oxygen between the cell and the nutrient phases of the averaging volume. The reaction rate kinetic function describing the overall oxygen consumption (for metabolic and growth processes) is assumed to follow Michaelis−Menten kinetics (*32*, *33*). Q_{m} and K_{m} are Michaelis−Menten parameters.

The effective diffusion coefficient accounts for the diffusion in the cellular and the nutrient (noncellular) phase as well as the mass transport between the two phases in the cell layer (*25*−*27*, *29*, *30*, *33*). Cell growth in the model is expressed in terms of the cell volume fraction (ϵ_γ), i.e., the volume occupied by cells in the averaging volume, V_γ, relative to the total averaging volume V in the cell layer. The sum of the volume fractions of the cell phase and the nutrient phase in the reactor is one (*25*).

Boundary Conditions. Oxygen flux at the upper boundary of the bulk liquid layer with the membrane is represented by the rate of mass transfer of oxygen from the incubator (saturated with oxygen in equilibrium with 21% oxygen, C_{atm}) through the FEP membrane (with permeability, *Perm*) into the bulk liquid. This boundary condition is written as

$$-D_\beta \frac{\partial c}{\partial y} = Perm(C_{\text{atm}} - c) \quad \forall x = [0,L]\ y = l + T \tag{4a}$$

The *Danckwerts* boundary condition, a flux balance at the inlet of the reactor coupled with a zero diffusive gradient condition at the end of the reactor (*35*), is used. These conditions are given by

$$v c_{\text{in}} = v c - D_\beta \frac{\partial c}{\partial x} \quad \forall y = [l, l + T]\ x = 0 \tag{4b}$$

$$D_\beta \frac{\partial c}{\partial x} = 0 \quad \forall y = [l, l + T]\ x = L \tag{4c}$$

where c_{in} is the dissolved oxygen concentration delivered by flow at the inlet. This is same as C_{atm}.

The equal diffusive flux condition exists at the interface of the cell layer and the liquid layer and is given as

$$-D_\beta \nabla c|_{\text{liquidlayer}} = -D_{\text{eff}} \nabla c|_{\text{celllayer}} \tag{4d}$$

It is assumed that there is no flux of oxygen along the external boundaries of the cell layer with the solid walls of the reactor. Hence,

$$\nabla D_{\text{eff}} c = 0 \quad \forall y = [0,l]\ x = 0 \tag{4e}$$

$$\nabla D_{\text{eff}} c = 0 \quad \forall y = [0,l]\ x = L \tag{4f}$$

$$\nabla D_{\text{eff}} c = 0 \quad \forall x = [0,L]\ y = 0 \tag{4f}$$

Unit 2 (Static Culture Unit). For the static culture unit there is no convective flow in both the bulk liquid layer and the cell layer. The effective area of supply of oxygen is reduced to one-half since the supply is only at the upper boundary of the construct. Similar to the perfusion Unit 1, material balances describing the oxygen transport and reaction are written in the bulk liquid layer and cell layer for this unit.

The continuity equations describing oxygen concentration variation due to diffusion in the bulk liquid layer and cell layer are written as

$$\frac{\partial c}{\partial t} = (\nabla D_\beta \nabla c) \qquad \text{bulk liquid layer} \tag{5}$$

$$\frac{\partial c}{\partial t} = \nabla D_{\text{eff}} \nabla c - \frac{Q_{\text{m}} K_{\text{eq}} \epsilon_\gamma c}{\frac{K_{\text{m}}}{C_{\text{o}}} + K_{\text{eq}} c \epsilon_\gamma} \qquad \text{cell layer}$$

Boundary Conditions. The oxygen concentration at the upper boundary of the bulk liquid layer is in equilibrium with 21% oxygen concentration in gas phase (C_{atm}). This boundary condition is written as

$$c = C_{\text{atm}} \quad \forall x = [0,L]\ y = 2l + T \tag{6a}$$

The equal flux condition exists at the interface of the cell layer and the liquid layer and is given as

$$-D_\beta \nabla c|_{\text{liquidlayer}} = -D_{\text{eff}} \nabla c|_{\text{celllayer}} \tag{6b}$$

As with the perfusion unit it is assumed here that there is no flux of oxygen along the external boundaries of the cell layer with the solid walls of the reactor. Hence,

$$\nabla D_{\text{eff}} c = 0 \quad \forall y = [0,l]\ x = 0 \tag{6c}$$

$$\nabla D_{\text{eff}} c = 0 \quad \forall y = [0,2l]\ x = L \tag{6d}$$

$$\nabla D_{\text{eff}} c = 0 \quad \forall x = [0,L]\ y = 0 \tag{6e}$$

Cell Growth Kinetics. Cell density is expressed in terms of the cell volume fraction (ϵ_γ) [fraction of volume occupied by cells in the averaging volume, V_γ, relative to the total averaging volume V] in the cell layer. The cell mass balance in the cell layer is written assuming exponential homogeneous growth and neglecting effects of oxygen on cell growth and occurrence of cell death as

$$\epsilon_\gamma = \epsilon_{\gamma o}\, e^{mt} \tag{7}$$

where $\epsilon_{\gamma o}$ is the initial cell volume fraction (computed from initial cell density) and m is the cell growth rate.

Parameter Estimation.

Metabolic Parameters. The specific oxygen consumption rate, Q_{m}, for the perfusion unit (Unit 1) is directly determined from experimental data as a quadratic function of time (Figure 6b). The cell growth in static and

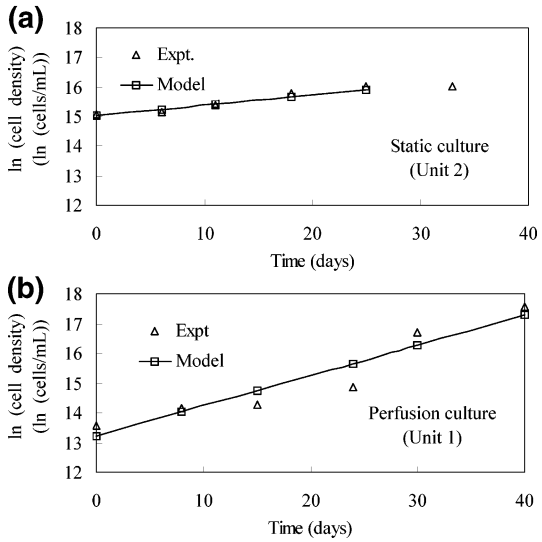

Figure 2. Growth kinetics of hMSCs under (a) static and (b) perfusion conditions.

perfusion culture units are seen to be similar for the first 24 days of culture. Hence Q_m for the static culture unit is obtained by averaging the oxygen consumption of the first three experimental data points obtained for the perfusion unit (Figure 6b). The K_m values of hMSCs have been reported to be in a similar range as that of other human cells, i.e., ca. 1.5−7.6 mmHg of the saturation oxygen tension (*32*, *34*). Therefore, a K_m value of $0.05C_o$ (7.6 mmHg) is chosen.

Cell Growth Parameters. The cell growth rates for hMSCs in perfusion and static culture units are determined by statistical methods only during the growth phase. Linear least-squares regression analysis is used to obtain the best-fit curve as shown in Figure 2 (*36*).

Table 1 outlines all the relevant parameters used in the model.

Solution Procedure. The equations describing variations in oxygen concentration in the liquid layer (eq 1) and in the cell layer (eq 3) and the cell growth (eq 7) in space and time were solved simultaneously coupled with the appropriate boundary conditions (eq 4) and growth parameters for perfusion culture Unit 1. For the static culture Unit 2, species continuity balances eq 5 coupled with specific growth kinetics were solved using the boundary conditions stated in eq 6. A MATLAB (version 6.5, The Mathworks, Inc.)-based FEMLAB (version 2.3, COMSOL) program utilizing a finite element method was used to numerically solve the system of partial differential equations. The oxygen concentration in both units at the initial time is set to C_{atm} (oxygen concentration in equilibrium with 21% oxygen in gas phase). The local oxygen concentrations obtained are macroscopically averaged to obtain the area averaged oxygen concentration as a function of time (*25*).

Results

Cell Growth Kinetics. The cell growth data were reported in a prior publication (*19*). HMSCs exhibited similar growth patterns in both static and perfusion cultures during the initial 24 days of culture. During this time period, cells displayed linear growth kinetics with the number of cells in the static culture increasing 260% (Figure 2a) and cells in the perfusion culture increasing 360% (Figure 2b). The difference in growth during the initial period was most probably due to variations in the initial seeding density. Higher cell seeding numbers resulted in lower growth rates in the static cultures, which is consistent with earlier reports of hMSCs' dependence on seeding density on 2-D surfaces (*22*) and in 3-D matrices (*20*). After day 24, cell numbers in the static cultures remained constant (Figure 2a). In the perfusion cultures, however, the cell numbers continued to increase exponentially, resulting in a total 50-fold increase by day 40 (Figure 2b). The exponential growth rate coefficient m is calculated as explained in Parameter Estimation to be 1.177×10^{-6} s^{-1} and 3.875×10^{-7} s^{-1} for the perfusion reactor (Unit 1) and the static culture (Unit 2) units, respectively. This value of the growth coefficient and the known initial cell density are used in eq 7 to obtain the cell growth function as shown in Figure 2.

Distribution of Proliferating Cells. BrdU assays were performed to locate the proliferating cells in the constructs. BrdU is a thymidine analogue that is incorporated into the DNA of proliferating cells during the S-phase of the cell-cycle and can be detected using antibodies conjugated to fluorescent probes. Figure 3a and b, respectively, show propidium iodide (PI) and BrdU staining of the hMSCs in an arbitrary view field of an hMSCs construct from the perfusion culture. There were no BrdU positive cells on both sides of the static culture constructs at day 7, correlating with the lag phase of cell growth. However, by day 21, there was a statistically significant increase in the number of BrdU positive cells in the upper (17.7%, the side contacting media) and lower (4.44%) surfaces of the constructs, indicating different growth patterns in the two surfaces (Figure 4a). At day 35, BrdU positive cells decreased to 7.3% in the upper surfaces and 3.1% in the lower surfaces ($p < 0.05$). By contrast, there is no significant difference in the growth patterns at the two surfaces of the constructs in the perfusion cultures ($p > 0.05$) (Figure 4b). At day 28, a comparable percentage of BrdU positive cells was found on the upper (17.2%) and lower (16.1%) surfaces of constructs under perfusion culture, which is also comparable with the BrdU positive cells on the upper surfaces of constructs under static culture at day 21 (17.7%). By day 38, the percentage of BrdU-incorporating cells dramatically decreased to 1.15% on the upper surfaces and 1.6% on the lower surfaces (Figure 4b).

Cellular Metabolism and Oxygen Consumption. Cellular metabolism rates were monitored by measuring the glucose and lactate concentrations. Although the rates of overall glucose consumption and lactate production in the static and perfusion cultures increased exponentially over the culture period, the metabolic rates in the static culture were always 1−2 orders of magnitude lower than those of the perfusion chambers (Figure 5a), while they increased in the perfusion reactor (Figure 5b). However, disparate culture conditions make the comparison of lactate-to-glucose ratios ($Y_{L/G}$) more meaningful: the average $Y_{L/G}$ values for static and perfusion cultures are 1.8 and 1.3, respectively (Figure 5c,d).

The specific oxygen consumption rates of hMSCs in the perfusion reactor were obtained by dividing the difference between oxygen concentrations measured at the inlets and outlets (Figure 6a) of the perfusion chambers by the cell number and the residence time of the media and were then normalized by the specific cell volume and equilibrium oxygen concentration; these are presented in Figure 6b. The oxygen consumption for the first 24 days of perfusion culture increased slightly, followed by a sharper increase from day 24 to day 35 and a subsequent decline from day 35 to day 40. The specific oxygen consumption rates were roughly constant for the first 24 days followed

Table 1. Parameters

parameter	value	reference
	Cellular Parameters	
specific cell volume	$V_g = 2.8 \times 10^{-9}$ cm^3/cell	Chow et al., 2001
metabolic parameters		
static		
dimensionless specific oxygen consumption rate	$Q_m = 0.002588$ 1/s	this work
saturation constant	$K_m = 1.105265 \times 10^{-8}$ mol/cm^3 (=$0.05C_o$)	Peng and Palsson, 1996; Chow et al., 2001a
perfusion		
dimensionless specific oxygen consumption rate	Q_m (1/s) = $(-3.6198 \times 10^{-16})t^2 + (6.6040 \times 10^{-10})t + 2.3413 \times 10^{-3}$	this work
saturation constant	$K_m = 1.105265 \times 10^{-8}$ mol/cm^3 (=$0.05C_o$)	Peng and Palsson, 1996; Chow et al., 2001a
growth parameters		
static		
cell growth rate	$m = 3.87454 \times 10^{-7}$ 1/s	this work
initial cell volume fraction	$\epsilon_{\gamma o} = 9.65 \times 10^{-3}$	this work
perfusion		
cell growth rate	$m = 1.18 \times 10^{-6}$ 1/s	this work
initial cell volume fraction	$\epsilon_{\gamma o} = 1.53 \times 10^{-3}$	this work
	Substrate Parameters	
Henry's coefficient for oxygen	$k_h = 0.95$ atm·L/mmol	Chow et al., 2001
oxygen concn in equilibrium with 20% gas-phase oxygen	$C_o = 2.10 \times 10^{-7}$ mmol/cm^3	Chow et al., 2001
oxygen diffusion coefficient in medium (liquid layer)	$D_\beta = 3.29 \times 10^{-5}$ cm^2/s	Chow et al., 2001
oxygen diffusion coefficient through cells in the matrix (in cell layer)	$D_\gamma = 1.59 \times 10^{-5}$ cm^2/s	Chow et al., 2001
	Averaging Volume Parameters	
radius of the averaging volume	$R = 50$ μm	Pathi et al., 2005
mass transfer coefficient at the interface of the cell and liquid region in the averaging volume	$P = 0.004$ cm/s $\alpha = (D_\gamma / L\,P) = 3.18$	Pathi et al., 2005
equilibrium coefficient	$K_{eq} = 1$ $k = (K_{eq} D_\gamma / D_\beta) = 0.48328$	Pathi et al., 2005
	Reactor Parameters	
static		
matrix thickness	$2l = 0.12$ cm	
liquid layer thickness	$T = 0.6$ cm	
reactor length	$L = 10$ cm	
reactor width	$w = 2.5$ cm	
perfusion		
matrix thickness	$2\,l = 0.12$ cm	
liquid layer thickness	$T = 0.6$ cm	
reactor length	$L = 10$ cm	
reactor width	$w = 2.5$ cm	
flow rate/chamber	0.1 mL/min = 1.67×10^{-3} cm^3/s	
average velocity	$v_{avg} = 1.11 \times 10^{-3}$ cm/s	
membrane characteristics		
FEP membrane		
thickness	130 μm	
length	10 cm	
membrane permeability	$Perm = 1.343 \times 10^{-5}$ cm/s	

by a decline up to day 40. A second-order polynomial equation was used to fit the specific oxygen consumption rate (as described in Parameter Estimation). The specific oxygen consumption rate used for static condition simulations was obtained by averaging the specific oxygen consumption rates over the first 24 days of the perfusion culture. The constructs in both perfusion and static conditions have comparable cell densities over the first 24 days and are assumed to have comparable oxygen consumption rates throughout this period (*37*, *38*).

Oxygen Profiles. The spatial and temporal variations of oxygen concentration in the cell layer and bulk liquid layer of the perfusion reactor (Unit 1) are shown in Figure 7a and b, respectively. The color represents the oxygen concentration variation in space, along the reactor length (from 0 to 10 cm) and thickness (from 0 to 0.66 cm). The oxygen concentration of the inlet flowing liquid was set to values in equilibrium with 21% gas-phase oxygen (which corresponds to the nondimensional value 1.05). The oxygen concentration decreased along with reactor depth and flow direction. The gradients in the liquid layer (Figure 7b) arise from diffusion and convective transport coupled to reaction, i.e., consumption by cells in the cell layer, which consumes oxygen at a faster rate than it can be supplied. Figure 7a shows the oxygen concentration variation in time and space for the flow Unit 1 in the cell layer. As the cells in the matrix (or the cell layer) grow exponentially, the highest oxygen consumption is to be expected at the later periods of time. However, during these times the specific oxygen consumption rate of these cells decreases considerably (as obtained from experimental data shown in Figure 6b), thus decreasing the total rate of oxygen consumption. This decrease in specific oxygen consumption rate and the large supply of oxygen by convective flow leads to an increase in the oxygen concentration around day 35.

For static culture (Unit 2), the calculated growth rate from the experimental data (Figure 2b) and oxygen consumption parameters as described are used to determine the oxygen concentration distribution. Oxygen concentration profiles in the bulk liquid layer and the cell layer are obtained as a function of space and time

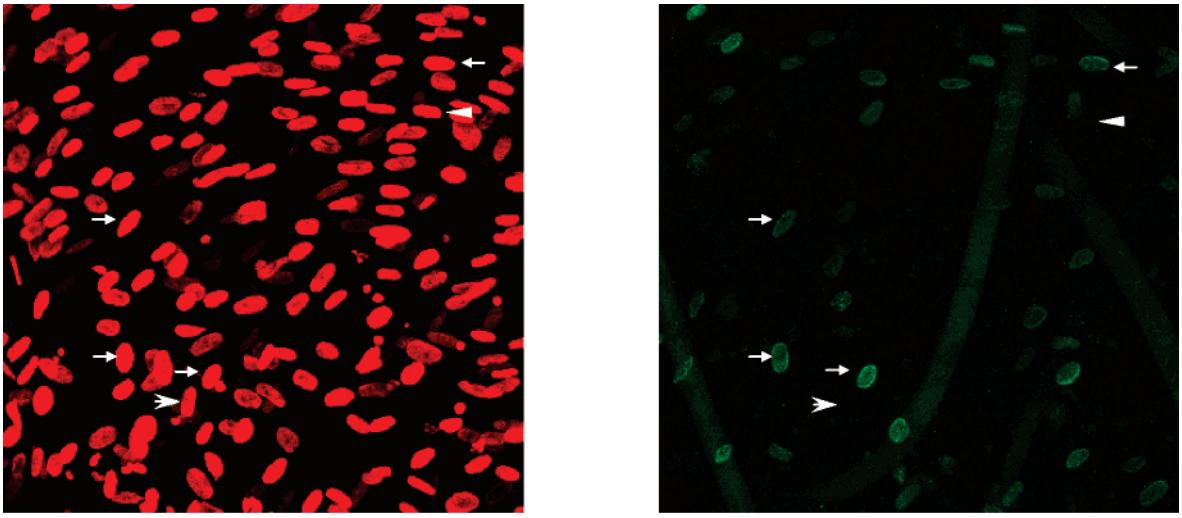

Figure 3. (a) Propidium iodide (PI) and (b) BrdU staining of hMSCs in an arbitrary view field of an hMSCs construct from perfusion culture. Arrows indicate examples of BrdU-positive cells. Arrowheads indicate examples of BrdU-negative cells.

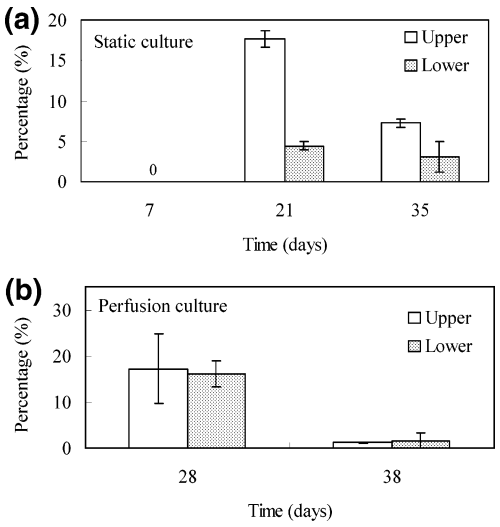

Figure 4. Percentage of BrdU positive cells on the surfaces of constructs under (a) static and (b) perfusion culture conditions.

for the no-flow Unit 2 (Figure 7c). Compared with the perfusion culture, this unit has a more uniform oxygen concentration distribution in space but a faster depletion during the whole culture time period. The larger depletion of oxygen in static culture (where it drops to a nondimensional value of 0.19) compared to the perfusion bioreactor (where it drops to a nondimensional value of 0.47) is attributed to the mode of oxygen supply, the surface area for oxygen supply, different cell growth kinetics, and the physiological differences in specific oxygen consumption in the two units.

The 2-D concentration profiles in the cell layer of the static (Figure 7c) and perfusion (Figure 7a) units are spatially averaged to obtain the macroscopically averaged oxygen consumption varying in time. As also seen in the spatial-temporal plots the averaged result shows that the oxygen concentration gradually decreased in the cell constructs or the cell layer both in static and perfusion units (Figure 8). However, the predicted depletion rate of oxygen in static culture unit is approximately double that of the perfusion unit, confirming that the presence of flow in liquid layer prevents the depletion of oxygen in the cell layer of the bioreactor throughout the course of the culture. The increase of the averaged oxygen level in both the bulk media and the cell constructs of the perfusion unit after 35 days are attributed to the decreased specific oxygen consumption rate and higher cell densities.

Discussion

High proliferation potential and plasticity make hMSCs attractive cell sources for tissue engineering applications. Sustaining a spatially uniform construct development at high cell density is an important aspect of hMSC tissue engineering. Results from this study show that culture environment has significant influences on cell growth and metabolisms, which are partially attributed to transport limitations in the static culture based on modeling analysis. The 3-D constructs grown in static cultures developed significant oxygen gradients and have the tendency to give rise to spatially nonuniform and inconsistent construct development, highlighting the need to optimize the culture environment for functional hMSC construct development.

Metabolism, Oxygen Tension, and Cell Proliferation. The key parameters affecting the glucose metabolism of animal cells are cell density and the glucose concentration in the culture (*39*, *40*). Although cells in both static and perfusion cultures display exponentially increased metabolic rates, the perfusion cultures exhibit 1−2 orders of magnitude higher glucose consumption and lactate production rates. The specific lactate production rate in the perfusion culture (2.39×10^{-12} g/cell·s) was ~70 times higher than in the static culture (3.35×10^{-14} g/cell·s) during the 4th week of culture. Similar trends were detected for specific glucose consumption rates. The unusually high metabolic activity of hMSCs is possibly indicative of the higher proliferative capabilities of the cells in the perfusion environment, where perfusion and timely media changes provides more effective nutrient delivery, and thus sustains an exponentially increasing nutrient demand especially at the later stage of the construct development. Additionally, oxygen limitations developed in the static culture may lead to different metabolic activities from the perfusion culture. The increased $Y_{L/G}$ ratio of 1.8 in the static cultures compared to the $Y_{L/G}$ ratio of 1.3 in the perfusion culture suggests

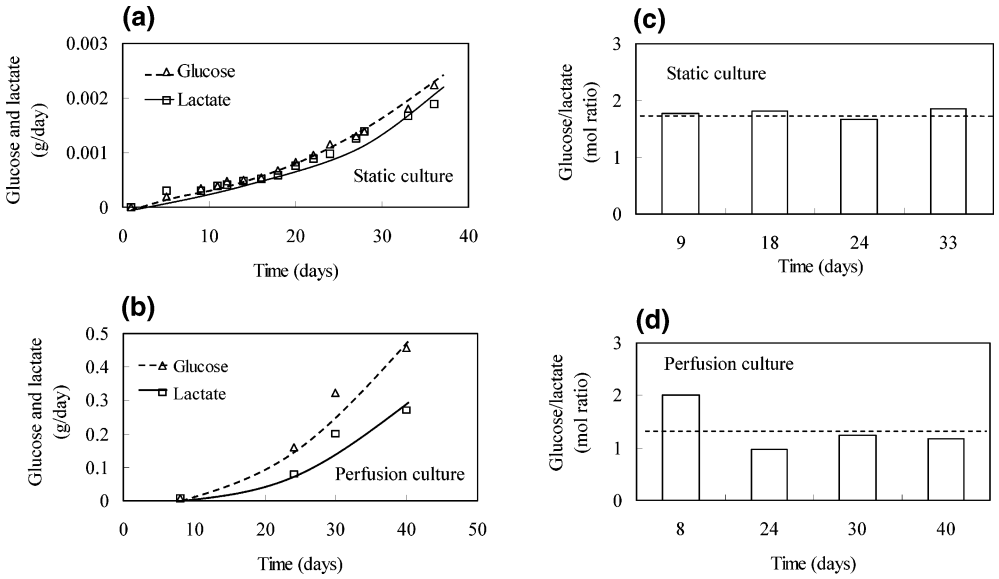

Figure 5. Total daily glucose consumption and lactate production of hMSCs over the 40-day culture period are shown for (a) static and (b) perfusion cultures. Ratios of lactate production and glucose consumption are also shown for (c) static and (d) perfusion. Dashed lines indicate average over the 40-day culture period.

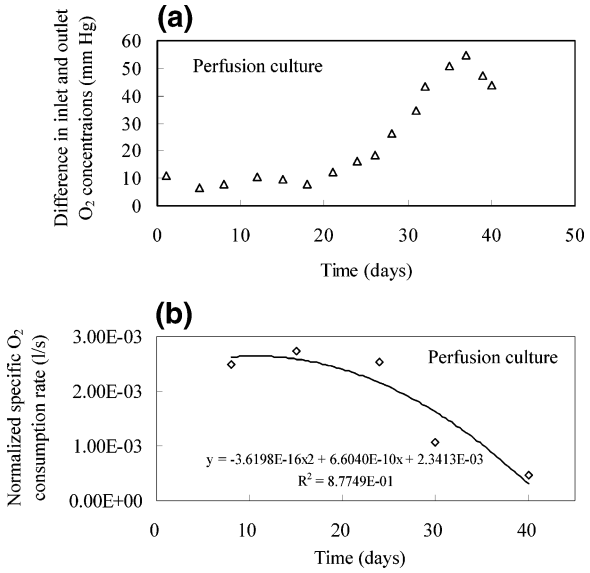

Figure 6. (a) Comparison of experimental with calculated values of the difference of oxygen concentration in inlet and outlet of the perfusion chambers. (b) Comparison of experimental and theoretical results of the normalized specific oxygen consumption rate throughout the culture period.

that cells experience a hypoxic environment in static condition (*40*, *41*).

Oxygen tension influences cellular events leading to the construct formation, including cell attachment and spreading (*42*, *43*), proliferation (*42*, *44*), migration (*45*), secretion of ECM (*46*, *47*), and differentiation (*48*, *49*). It appears that the cell proliferation patterns in the static culture ($p < 0.05$) correlate to the oxygen distribution along the vertical direction, whereas no significant difference in the growth patterns at the two surfaces of the constructs was observed in the perfusion culture, ($p > 0.05$). In the static culture, the lowest nondimensional oxygen level in the cell layer decreased from nearly 0.5 (~10% gas-phase oxygen) in the initial phase (around 10 days) of the culture period to nearly 0.19 (~3.8% gas-phase oxygen) at end of the culture period (around 40 days), whereas in the perfusion unit the lowest level of oxygen tension in the construct was maintained above 0.47 (~9.4% gas phase oxygen) throughout the culture period even at the highest cell densities. Experimental studies have shown that the effects of oxygen tension on cell proliferation and ECM secretion are significant only when the oxygen tension is lower than 40 mmHg (*50*), which corresponds to the dimensionless oxygen tension of 0.26 (~5.3% gas-phase oxygen) in this study. Therefore, it is reasoned that the oxygen level in the constructs of the perfusion bioreactor system (Unit 1) is maintained above the level that could lead to significant cellular physiological changes, whereas the oxygen distribution might limit the cell growth and metabolism of the constructs in static culture (Unit 2).

Various mathematical modeling approaches have been developed to correlate and predict the effects of oxygen distribution on cell proliferation and tissue development. Efforts have been made to model solute transport and cell growth kinetics for chondrocyte cells in constructs placed in bioreactor units (*51*–*55*). The limitations of these models, however, are that the nutrient transport is not coupled with the increase in cell mass due to growth and formation of ECM and that they do not incorporate the effects of the restricted diffusion of nutrients on the chondrocyte activity (*51*, *52*, *54*). Our model utilizes the method of volume averaging to study growth kinetics of hMSCs, oxygen transfer restrictions, and temporal variation of cell mass within the PET matrix in the static and perfusion units. The unique feature of the model is that it determines the effective diffusion and reaction coefficients to account for restrictions due to the formation of cell mass and mass transfer limitations. The model utilizes the available experimental data on specific oxygen consumption and cell growth to determine the spatial and temporal oxygen profiles of static and perfusion units.

It is important to note, however, that oxygen tension may not be the only factor that influences cell spatial growth pattern. In addition to oxygen, diffusion also limits other nutrients delivery and waste removal in the static culture that hinders cell growth. Moreover, the medium flow and shear stress also influence cell proliferation in the perfusion culture (*56*) and the expression of differentiation markers by MSCs (*56*–*59*). While the flow rate of 0.1 mL/min ($Re = 0.28$) used in this study is

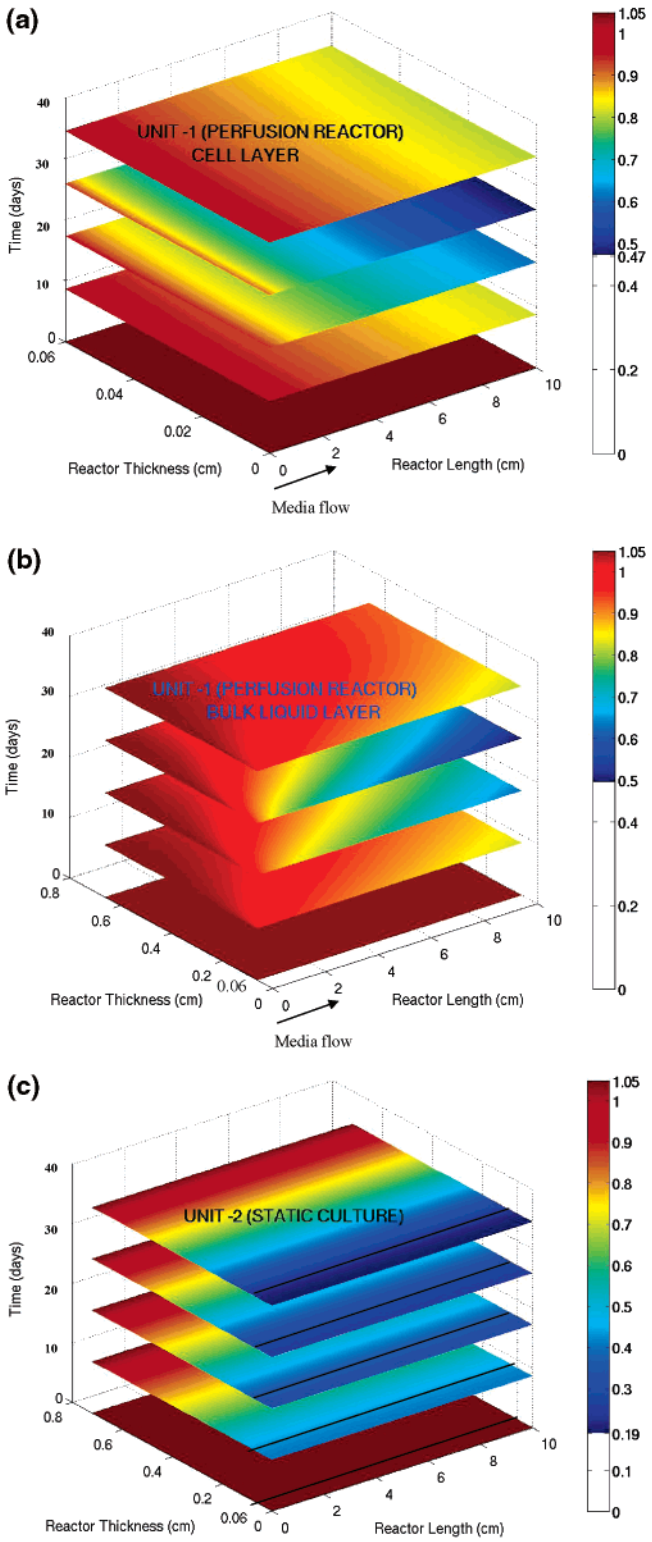

Figure 7. Mathematical simulation of the spatio-temporal variation of oxygen concentration in the cell layer (a) and bulk liquid layer (b) in perfusion chamber; and cell layer and bulk liquid layer in static culture (c).

sufficiently low compared to these studies ($Re \approx 50$), further investigation using different flow rate is necessary to independently elucidate the effects of shear force.

Specific Oxygen Consumption at High Cell Density. The specific oxygen consumption rate is an important parameter in determining the transport characteristics of the bioreactor system and in bioreactor design. The specific oxygen consumption rate in our study is

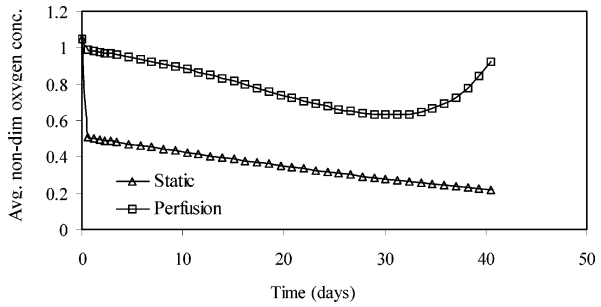

Figure 8. Average nondimensional oxygen concentration variations in cell layer with time for static and perfusion culture units.

calculated in a range of 0.0017−0.012 μmol/10^6 cells/h which is in a comparable range as reported for chondrocytes and hepatocytes (*37*, *38*). It is interesting to note that the specific oxygen consumption rate of hMSCs is not a constant value and decreased to one-fifth of the highest value as the cell density increased in the perfusion culture. A similar dependence of specific oxygen consumption rate on cell density in the 3-D construct was reported in the hepatocyte culture when grown in 3-D constructs (*38*). Isolated hepatocytes grown on monolayer culture also have an order of magnitude higher oxygen consumption rate compared to the cells grown in the 3-D constructs, and chondrocytes grown in the 3-D construct have a lower specific oxygen consumption rate (*37*, *38*). It may be argued that diffusion limitations cause the decreased specific oxygen consumption rate at high cell density, i.e., day 40. However, a sharp decrease is observed at day 30 when the ratio of oxygen consumed is less than 20% of inlet oxygen level, which is unlikely in the region of diffusion control. For the case of hepatocytes grown in a hollow fiber bioreactor, it is suggested that high cell density in 3-D system approximates that in a natural tissue configuration and therefore cells are less stressed and have lower specific oxygen consumption rate. The sharp decrease observed in our study may be an indicator that intrinsic physiological changes occur at high cell density in 3-D hMSC constructs. The decreasing specific oxygen consumption rates lead to the decreased total oxygen consumption at a later stage of perfusion culture when the cell density approaches 10×10^6 cell/mL. These findings challenge the convention that the specific oxygen consumption rate depends on oxygen tension but is independent of cell density and suggest that the design parameters for the perfusion system are not transferable from monolayer cultures and must be independently obtained with 3-D culture systems. Model simulation, used in conjunction with the simple design of the perfusion system as illustrated in this study, reveals physiological aspects of construct development and is an integral part of developing optimal strategy for the development of tissue constructs with desired structural and biological characteristics.

Conclusions

Recent studies have demonstrated that signals transmitted to cells in 3-D environments cannot be suitably mimicked during culture on flat surfaces, and cells undergo different tissue-development processes in 3-D culture (*60*). Cell survival, as well as proliferation, differentiation, and ECM secretion, are all controlled by the spatial organization of cells (*61*, *62*). Utilization of 3-D scaffolds is a central part of tissue engineering strategy and plays an essential role for functional tissue

constructs production. As the importance of 3-D scaffolds is recognized and extensively studied, the current experimental and modeling study demonstrates the limitations of static 3-D culture systems and indicates that the oxygen transport has significant influences on cell proliferation and metabolic activities. The effects of the culture parameters may be more pronounced for hMSC tissue development because they are sensitive to the environmental cues and have high proliferation potential and plasticity. There is a recognizable need to improve the current system to further understand and to optimize the biological and physiological developmental patterns.

Acknowledgment

We gratefully acknowledge financial supports from American Cancer Society, Florida Division (F02S-FSU-1) and Florida State University Program Enhancement Award.

Notation

Flow Parameters

v_x	velocity vector of medium flow; cm/s
v_{ave}	average velocity of medium flow; cm/s
x	coordinate in the direction of flow
y	coordinate perpendicular to the direction of flow
l	half the height of the matrix; cm
L	length of the reactor/static unit; cm
T	height of the liquid layer in the bioreactor; cm
w	width of the bioreactor; cm

Growth Parameters

V	averaging volume; cm^3
V_i	volume occupied by cells in the ith phase ($i = \beta, \gamma$); cm^3
ϵ_γ	cell volume fraction $= V_\gamma/V$
ϵ_β	fluid volume fraction in cell layer
$\epsilon_{\gamma o}$	initial cell volume fraction (corresponding to initial cell density)
m	cell growth rate; 1/s

Metabolic Parameters

V_g	specific cell volume; cm^3/cell
C_o	dissolved oxygen concentration in equilibrium with the saturated oxygen concentration in air (20%); mol/cm^3
C_{atm}	dissolved oxygen concentration in equilibrium with the saturated oxygen concentration in air (21%), $1.05C_o$; mol/cm^3
Q_{mm}	specific oxygen uptake rate (metabolism); mol/cell/s
Q_m	normalized specific oxygen consumption rate $= Q_{mm}/(V_g C_o)$; 1/s
K_m	Michaelis–Menten saturation constant for metabolic oxygen consumption; mol/cm^3

Diffusion Constants

D_i	diffusion coefficient in the ith phase ($i = \beta, \gamma$); cm^2/s
D_{eff}	effective diffusion coefficient; cm^2/s
K_{eq}	equilibrium coefficient for oxygen between the β and the γ phases of the averaging volume
c	nondimensional oxygen concentration in cell layer $= C/C_o$
t	time; s

Boundary Condition Parameters

$Perm$	permeability FEP membrane; cm/s
c_{in}	dissolved oxygen concentration being delivered by flow at the inlet

References and Notes

(1) Horwitz, E. M.; Prockop, D. J.; Fitzpartick, L. A.; Koo, W. W.; Gordonm, P. L.; Neel, M.; Sussman, M.; Orchard, P.; Marx, J. C.; Pyeritz, R. E.; Brenner, M. K. Transplantability and therapeutic effects of bone marrow-derived mesenchymal cells in children with osteogenesis imperfecta. *Nat. Med.* **1999**, *5*, 309–313.

(2) Prockop, D. J. Marrow stromal cells as stem cells for nonhematopoietic tissues. *Science* **1997**, *276*, 71–74.

(3) Chen, J. L.; Li, Y.; Zhang, R. L.; Katakowski, M.; Gautam, S. C.; Xu, Y. X.; Lu, M.; Zhang, Z. G.; Chopp, M. Combination therapy of stroke in rats with a nitric oxide donor and human bone marrow stromal cells enhances angiogenesis and neurogenesis. *Brain Res* **2004**, *1005*, 21–28.

(4) Chen, J. L.; Zhang, Z. G.; Li, Y.; Wang, L.; Xu, Y. X.; Gautam, S. C.; Lu, M.; Zhu, Z.; Chopp, M. Intravenous administration of human bone marrow stromal cells induces angiogenesis in the ischemic boundary zone after stroke in rats. *Circ. Res.* **2003**, *92*, 692–699.

(5) Orlic, D.; Kajstura, J.; Chimenti, S.; Jakoniuk, I.; Anderson; S. M.; Li, B. S.; Pickel, J.; McKay, R.; Nadal-Ginard, B.; Bodine, D. M.; Leri, A., Anversa, P. Bone marrow cells regenerate infarcted myocardium. *Nature* **2001**, *410*, 701–705.

(6) Bancroft, G. N.; Sikavitsas, V. I.; Mikos, A. G. Design of a flow perfusion bioreactor system for bone tissue-engineering applications. *Tissue Eng.* **2003**, *9*, 549–554.

(7) Bancroft, G. N.; Sikavitsas, V. I.; van den Dolder, J.; Sheffield, T. L.; Ambrose; C. G.; Jansen, J. A.; Mikos, A. G. Fluid flow increases mineralized matrix deposition in 3D perfusion culture of marrow stromal osteoblasts in a dose-dependent manner. *Proc. Natl. Acad. Sci. U.S.A.* **2002**, *99*, 12600–12605.

(8) Cartmell, S. H.; Porter, B. D.; Garcia, A. J.; Guldberg, R. E. Effects of medium perfusion rate on cell-seeded three-dimensional bone constructs in vitro. *Tissue Eng.* **2003**, *6*, 1197–1203.

(9) Freed, L. E.; Vunjak-Novakovic, G. Cultivation of cell-polymer tissue constructs in simulated microgravity. *Biotechnol. Prog.* **1995**, *46*, 306–313.

(10) Freed, L. E.; Vunjak-Novakovic, G.; Marquis, J. C.; Langer, R. Kinetics of chondrocytes growth in cell-polymer implants. *Biotechnol. Bioeng.* **1994**, *43*, 597–604.

(11) Saini, S.; Wick, T. M. Concentric cylinder bioreactor for production of tissue engineered cartilage: effect of seeding density and hydrodynamic loading on construct development. *Biotechnol. Prog.* **2003**, *19*, 510–521.

(12) Williams, K. A.; Saini, S.; Wick, T. M. Computational fluid dynamics modeling of steady-state momentum and mass transport in a bioreactor for cartilage tissue-engineered. *Biotechnol. Prog.* **2002**, *18*, 951–963.

(13) Gooch, K. J.; Kwon, J. H. Blunk, T.; Langer, R.; Freed, L. E.; Vunjak-Novakovic, G. Effects of mixing intensity on tissue-engineered cartilage. *Biotechnol. Bioeng.* **2001**, *72*, 402–407.

(14) Vunjak-Novakovic, G.; Obradovic, B.; Martin, I.; Bursac, P. M.; Langer, R.; and Freed, L. E. Dynamic cell seeding of polymer scaffolds for cartilage tissue engineering. *Biotechnol. Prog.* **1998**, *14*, 193–202.

(15) Pei, M.; Solchaga, L. A.; Seidel, J.; Zeng, L.; Vunjak-Novakovic, G.; Caplan; A. I.; Freed, L. E. Bioreactors mediate the effectiveness of tissue engineering scaffolds. *FASEB. J.* **2002**, *16*, http://www.fasebj.org/cgi/reprint/02–0083fjev1.pdf.

(16) Jasmund, I.; Langsch, A.; Simmoteit, R.; Bader, A. Cultivation of primary porcine hepatocytes in an OXY-HFB for use as a bioartificial liver device. *Biotechnol. Prog.* **2002**, *18*, 839–846.

(17) Wendt, D.; Marsano, A.; Jakob, M.; Heberer, M.; Martin, I. Oscillating perfusion of cell suspensions through three-

dimensional scaffolds enhances cell seeding efficiency and uniformity. *Biotechnol. Bioeng.* **2003**, *84*, 205−214.
(18) Sikavitsas, V. I.; Bancroft, G. N.; Holtorf, H. L.; Jansen, J. A.; Mikos, A. G. Mineralized matrix deposition by marrow stromal osteoblasts in 3D perfusion culture increases with increasing fluid shear forces. *P. Natl. Acad. Sci. U.S.A.* **2003**, *100*, 14683−14688.
(19) Zhao, F.; Ma, T. Perfusion bioreactor system for human mesenchymal stem cell tissue engineering: dynamic cell seeding and constructs development. *Biotechnol. Bioeng.* **2005**, Early View DOI: 10.1002/bit.20532.
(20) Grayson, W. L.; Ma, T.; Bunnel, B. Human mesenchymal stem cells tissue development in 3D PET matrices. *Biotechnol. Prog.* **2004**, *20*, 905−912.
(21) DiGirolamo, C. M.; Stokes, D.; Colter, D.; Phinney, D. G.; Class, R.; Prockop, D. J. Propagation and senescence of human marrow stromal cells in culture: a simple colony forming assay identifies samples with the greatest potential to propagate and differentiate. *Br. J. Haematol.* **1999**, *107*, 275−281.
(22) Sekiya, I.; Larson, B. L.; Smith, J. R.; Pochampally, R.; Cui, J. G.; Prockop, D. J. Expansion of human adult stem cells from bone marrow stroma: conditions that maximize the yields of early progenitors and evaluate their quality. *Stem Cells* **2002**, *6*, 530−541.
(23) Li, Y.; Ma, T.; Kniss, D. A.; Yang, S. T. Modification and characterization of PET non-woven fibrous matrix as cell culture scaffold. *Biomaterials* **2001**, *22*, 609−618.
(24) Ma, T.; Li, Y.; Yang, S. T.; Kniss, D. Effects of trophoblast cell organization in fibrous matrix on long-term tissue development and cell cycle. *Biotechnol. Bioeng.* **2000**, *70*, 606−618.
(25) Pathi, P.; Ma, T.; Locke, B. R. Role of nutrient supply on cell growth in bioreactor design for tissue engineering of hematopoietic cells. *Biotechnol. Bioeng.* **2005**, *89*, 743−758.
(26) Galban, C. J.; Locke, B. R. Analysis of cell growth kinetics and substrate diffusion in a polymer scaffold. *Biotechnol. Bioeng.* **1999**, *65*, 121−132.
(27) Galban, C. J.; Locke, B. R. Effects of spatial variation of cells and nutrient and product concentrations coupled with product inhibition on cell growth in a polymer scaffold. *Biotechnol. Bioeng.* **1999**, *64*, 633−643.
(28) Whitaker, S. *The Method of Volume Averaging−Theory and Applications of Transport in Porous Media*; Kluwer Academic Publishers: Norwell, 1999.
(29) Wood, B. D.; Quintard, M.; Whitaker, S. Calculation of effective diffusivities for biofilms and tissues. *Biotechnol. Bioeng.* **2002**, *77*, 495−516.
(30) Wood, B. D.; Whitaker, S. Multi-species Diffusion and reaction in biofilms and cellular media. *Chem. Eng. Sci.* **2000**, *55*, 3397−3418.
(31) Ochoa, J. Diffusion and reaction in heterogeneous media. Ph.D. Dissertation, University California Davis, 1988.
(32) Chow, D. C.; Wenning, L. A.; Miller, W. M.; Papoutsakis, E. T. Modeling pO_2 distributions in the bone marrow hematopoietic compartment. I. Krogh's Model. *Biophys. J.* **2001**, *81*, 675−684.
(33) Chow, D. C.; Wenning, L. A.; Miller, W. M.; Papoutsakis, E. T. Modeling pO_2 distributions in the bone marrow hematopoietic compartment. II. Modified Krogh's Models. *Biophys. J.* **2001**, *81*, 685−696.
(34) Peng, C. A.; Palsson, B. O. Determination of specific oxygen uptake rates in human hematopoietic cultures and implications for bioreactor designs. *Ann. Biomed. Eng.* **1996**, *24*, 373−381.
(35) Danchwerts, P. V. Continuous flow systems. *Chem. Eng. Sci.* **1953**, *2*, 1−13.
(36) NIST/SEMATECH e-Handbook of Statistical Methods, http://www.itl.nist.gov/div898/handbook/, section 4.1.4.1.
(37) Malda, J.; Rouwkema, J.; Martens, D. E.; le Comte, E. P.; Kooy, F. K.; Tramper, J.; van Blitterswijk, C. A.; Riesle, J. Oxygen gradients in tissue-engineered PEGT/PBT cartilaginous constructs: Measurement and modeling. *Biotechnol. Bioeng.* **2004**, *86*, 9−18.
(38) Patzer, J. F. Oxygen consumption in a hollow fiber bioartificial liver−revisited. *Artif Organs* **2004**, *28*, 83−98.
(39) Linz, M.; Zeng, A. P.; Wagner, R.; Deckwer, W. D. Stoichiometry, kinetics, and regulation of glucose and amino acid metabolism of a recombinant BHK cell line in batch ad continuous cultures. *Biotechnol. Prog.* **1997**, *13*, 453−463.
(40) Zeng, A. P.; Hu, W. S.; Deckwer, W. D. Variation of stoichiometric ratios and their correlation for monitoring and control of animal cell cultures. *Biotechnol. Prog.* **1998**, *14*, 434−441.
(41) Zauner, A.; Clausen, T.; Alves, O. L.; Rice, A.; Levasseur, J.; Young, H. F.; Bullock, R. Cerebral metabolism after fluid-percussion injury and hypoxia in a feline model. *J. Neurosurg.* **2002**, *97*, 643−649.
(42) Mitchell, S. A.; Poulsson, A. H. C.; Davidson, M. R.; Emmison, N.; Shard, A. G.; Bradley, R. H. Cellular attachment and spatial control of cells using micro-patterned ultraviolet/ozone treatment in serum enriched media. *Biomaterials* **2004**, *25*, 4079−4086.
(43) Rotem, A.; Toner, M.; Bhatia, S.; Foy, B. D.; Tompkins, R. G.; Yarmush, M. L. Oxygen is a factor determining in vitro tissue assembly: Effect on attachment and spreading of hepatocytes. *Biotechnol. Bioeng.* **1994**, *43*, 654−660.
(44) Duggan, O.; Hyland, P.; Annett, K.; Freeburn, R.; Barnett, C.; Pawelec, G.; Barnett, Y. Effects of a reduced oxygen tension culture system on human T cell clones as a function of in vitro age. *Exp. Gerontol.* **2004**, *39*, 525−530.
(45) Annabi, B.; Lee, Y. T.; Turcotte, S.; Naud, E.; Desrosiers, R. R.; Champagne, M.; Eliopoulos, N.; Galipeau, J.; Beliveau, R. Hypoxia promotes murine bone-marrow-derived stromal cell migration and tube formation. *Stem Cells* **2003**, *21*, 337−347.
(46) Chen, C. P.; Aplin, J. D. Placental extracellular matrix: Gene expression, deposition by placental fibroblasts and the effect of oxygen. *Placenta* **2003**, *24*, 316−325.
(47) Gebb, S. A.; Jones, P. L. Hypoxia and lung branching morphogenesis. *Adv. Exp. Med. Biol.* **2003**, *543*, 117−125.
(48) Cipolleschi, M. G.; Sbarba, P. D.; Olivotto, M. The role of hypoxia in the maintenance of hematopoietic stem cells. *Blood* **1993**, *82*, 2031−2037.
(49) Terai, H.; Hannouche, D.; Ochoa, E.; Yamano, Y.; Vacanti, J. P. In vitro engineering of bone using a rotational oxygen-permeable bioreactor system. *Mat. Sci. Eng., C* **2002**, *S 20*, 3−8, Sp. Iss. SI.
(50) Jiang, B.; Semenza, G. L.; Bauer, C.; Marti, H. H. Hypoxia Inducible Factor 1 levels vary exponentially over a physiologically relevant range of O_2 tension. *Am. J. Phys*. **1996**, *271*, C1172−C 1180.
(51) Nehring, D.; Adamietz, P.; Meenen, N.; Portner, R. Perfusion cultures and modeling of oxygen uptake with three-dimensional chondrocyte pellets. *Biotechnol. Tech.* **1999**, *13*, 701−706.
(52) Obradovic, B.; Meldon, J. H.; Freed, L. E.; Vunjak-Novakovic, G. Glycosaminoglycan deposition in engineered cartilage: experiments and mathematical model. *AlChE J.* **2000**, *46*, 1860−1871.
(53) Carrier, R. L.; Rupnick, M.; Langer, R.; Schoen, F. J.; Freed, L. E.; Vunjak-Novakovic, G. Perfusion improves tissue architecture of engineered cardiac muscle. *Tissue Eng.* **2002**, *8*, 175−188.
(54) Pisu, M.; Lai, N.; Cincotti, A.; Delogu, F.; Cao, G. A simulation model for the growth of tissue engineered cartilage on polymeric scaffolds. *J. Chem. React. Eng*. **2003**, *1*, http://www.bepress.com/ijcre/vol1/A38.
(55) Pisu, M.; Lai, N.; Cincotti, A.; Concas, A.; Cao, G. Modeling of engineered cartilage growth in rotating bioreactors. *Chem. Eng. Sci.* **2004**, *59*, 5035−5040.
(56) Li, Y. J.; Batra, N. N.; You, L.; Meier, S. C.; Coe, I. A.; Yellowley, C. E.; Jacobs, C. R. Oscillatory fluid flow affects human marrow stromal cell proliferation and differentiation. *J. Orthop. Res.* **2004**, *22*, 1283−1289.
(57) Park, J. S.; Chu, J. S. F.; Cheng, C.; Chen, F.; Chen, D.; Li, S. Differential effects of equiaxial and uniaxial strain on mesenchymal stem cells. *Biotechnol. Bioeng.* **2004**, *88*, 359−368.
(58) Meinel, L.; Karageorgiou, V.; Fajardo, R.; Snyder, B.; Shinde-Patil, V.; Zichner, L.; Kaplan, D.; Langer, R.; Vunjak-Novakovic, G. Bone tissue engineering using human mesen-

chymal stem cells: Effects of scaffold material and medium flow. *Ann. Biomed. Eng.* **2004**, *32*, 112−122.
(59) Sikavitsas, V. I.; Bancroft, G. N.; Mikos, A. G. Formation of three-dimensional cell/polymer constructs for bone tissue engineering in a spinner flask and a rotating wall vessel bioreactor. *J. Biomed. Mater. Res.* **2002**, *62*, 136−148.
(60) Cukierman, E.; Pankov, R.; Stevens, D. R.; Yamada, K. M. Taking cell−matrix adhesions to the third dimension. *Science* **2001**, *294*, 1708−1712.
(61) Yamada, K. M.; Clark, K. Cell biology−Survival in three dimensions. *Nature* **2002**, *419*, 790−791.
(62) Zahir, N.; Weaver, V. M. Death in the third dimension: apoptosis regulation and tissue architecture. *Curr. Opin. Genet. Dev.* **2004**, *14*, 71−80.

Accepted for publication May 24, 2005.

BP0500664